NiO@Pt/C Core-Shell Nanocatalyst for Oxygen Reduction Reaction

D. Vega-Villalobos[1], F. Godínez-Salomón[1], J. L. Reyes-Rodríguez[1], L. Lartundo-Rojas[2], O. Solorza-Feria[1*].

[1]Departamento de Química, Centro de Investigación y Estudios Avanzados del IPN, Av. IPN 2508, Col. San Pedro Zacatenco, A. Postal 14-740, 07360 México D.F., México.[2]Centro de Nanociencias y Micro y Nanotecnologías-IPN, UPALM, Col. San Pedro Zacatenco; A. Postal 07738 México D.F., México.
[*]Tel: 011 +52 +55 5747-3715 ; e-mail: osolorza@cinvestav.mx

ABSTRACT

In this work, we present the synthesis, as well physical and electrochemical characterization of the nickel oxide supported in Ketjenblack carbon decorated platinum core-shell nanocatalyst for the oxygen reduction reaction (ORR) in acid media. The core was synthesized by chemical reduction with $NaBH_4$ of $Ni(NO_3)_2.6H_2O$, while the shell was deposited by galvanic displacement on the surface of Ni nanoparticles. The presence of Pt in the core was proved by XRD. On the other hand, TEM micrographs have showed highly dispersed nanoparticles with an average between 2-20nm. The presence of Ni and Pt on 71 and 29 wt. % respectively was confirmed by EDAX while XPS and Raman spectroscopy confirms the presence of NiO. The electrochemical performance of NiO@Pt/C is evaluated by cyclic voltammetry, CO stripping and using rotating disk electrode setup, was carried out for the ORR in HClO4 electrolyte; indicated that have more catalytic activity than that of commercial 20% Pt / C-Etek® catalyst, used as reference.

Keywords: NiO:Pt core-shell nanoparticles; oxygen reduction reaction, electrochemical analysis.

1. Introduction

Increasing energy demands have stimulated intense research on alternative energy conversion and storage systems with high efficiency, low cost and environmental benignity. That's why has generated substantial interest in electrochemical energy conversion, particularly in fuel cells and therefore has generated vigorous investigation of the oxygen reduction reaction (ORR) on a wide range of materials Pt-based [1-2].

One important part of the fuel cells is the catalysts, but Pt is expensive and increases the price of this. The proposed is reducing the amount of the noble metal, therefore Pt-alloyed with various transition metals are employed to further improve the electrocatalytic activity of ORR and reduce the cost of electrocatalyst. So the responsible for the surface catalytic reactivity might be at on reduced Pt-Pt distance near the particle surface stabilized by the lattice contracted alloy core, i.e. the presence of transition metal located within the core due to the structure and electronic effects caused by the partial alloying and vacant d-orbital from the transition metal, and the dissolution of the transition metal is expectably reduced due to the protection by Pt on the shell [3-6].

An ideal electrocatalysts for ORR would be capable of activating molecular O_2 while at the same time not binding oxygen intermediates, O*, OH* and OOH*, so strongly as to inhibit their reduction to water[7]. The ORR on Pt and Pt-family metals occurs by the parallel mechanism following predominantly a direct four-electron reduction (see Fig. 1); little hydrogen peroxide is generated, particularly when some adventitious impurities contaminated the electrode surface [6-8].

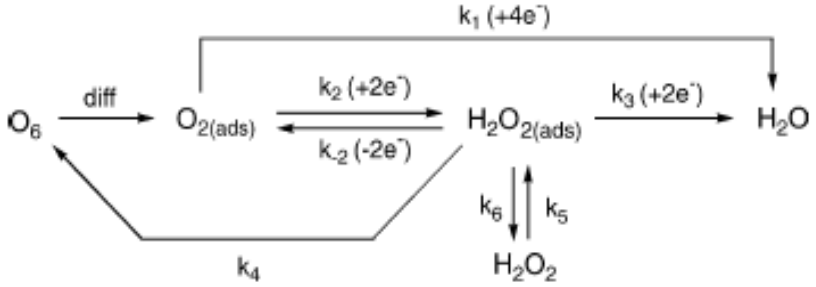

Fig.1 Reaction Mechanism of the ORR, taken from the reference [8].

There were many reports on the fabrication of core–shell particles, such as electrochemical method, electroless plating, layer-by-layer deposition, laser pulses, self-assembly, chemical reduction, microwave synthesis, sonochemical method, decomposition of organometallic precursors and photoreduction [9].

2. Experimental

2.1. Material synthesis.

The electrocatalytic material was synthesized by modified Bönnemann procedure [10]. First the precursor salt $Ni(NO_3)_2$* $6H_2O$ and the capping agent Tetrabutyl ammonium hydroxide (TBAOH) in

molar ratio 1:1, were dissolved in 60 ml of ethanol and magnetically stirred during 19 h at room temperature. Then the agent reduction $NaBH_4$ in molar ratio 1:6 with respect at precursor; dissolved in 40 ml of ethanol was added drop by drop, using a ultrasonic lance, with the potency of 20kHz ±50 Hz and with a period of 30 seconds ON and 10 seconds OFF for 90 minutes. The core was supported on carbon Ketjenblack, estimating a 50% metal loading expressed as a weight. The NiO@Pt/C core-shell catalyst was prepared by galvanic replacement, mixing Ni:Pt ratio of 85:15. [11-12]

2.2. Electrochemical characterization

The electrochemical measurements were conducted at room temperature in a typical three electrodes cell filled with 0.1M $HClO_4$ electrolyte solution; using a rotating disk electrode (RDE) setup with a potenciostat /galvanostat (PARSTAT model 2273). The electrochemical cell and the working electrode were prepared according to Garsany et al. [13] Nominal Pt loading around 23 µg cm^2_{geo} were used. In the cyclic voltammetry the potential was cycled between 0.05 V and 1.2 V to obtain a stable voltammogram in a nitrogen-saturated 0.1M $HClO_4$. Electrochemical surface area was determinate by Co stripping techniques according to Markovic et al. [14]. Using the thin.-film disk electrode method [11-12,15], were determined of the parameters kinetic for the ORR. For this, the solution electrolyte was saturated with oxygen; the measurement was performed in a backward manner from 1.05 V to 0.05 V at 20 mV s^{-1}, maintaining the starting potential during 50 seconds before scanning.

2.3 X-ray diffraction

Crystal structure identification was performed by X-ray diffraction (XRD) using a diffractometer (PAN-analytical R&D Empyrean) whit monochromatic Cu-Kα radiation (λ= 1.5405 Å) in a 2θ range from 5° to 100°. Was analyzed the diffractogram using the Match 2 software.

2.4 Transmission electron microscopy (TEM)

Particle size, morphology and distribution were evaluated through transmission electron microscopy (TEM) using a JEM ARM200F instrument operated at an accelerated voltage of 300 kV. Nanoparticles size distribution was calculated based on a random counting of particles using the Image J software.

2.5 Energy dispersive X-ray analysis (EDAX)

The elemental mapping of the NiO@Pt catalysts were determined by the EDAX technique coupled to a scanning electron microscopy by AURIGA-39-16 applying 10 kV.

2.6 Raman spectroscopy

Raman spectra were recording using a Lap Ram HR800, Horiba Join Yvon, with a beam aperture of Pinhole of 400µm and 150 µm of Slit. The spectra are measurement from 0 to 4500 cm^{-1}.

2.7 X-ray photoelectron spectroscopy (XPS)

The XPS analyses were carried out with a Kratos Axis Ultra spectrometer using a monochromatic Al Kα source (*hv* = 1486.6 eV). The signal C1s was used with reference for the analyses. For the deconvolution of the spectra, was used the free program XPS Peak Fit 4.1.

3. Results and discussion

3.1 Physical characterization

3.1.1 X-ray diffraction (XRD)

Fig. 2 displays the XRD-pattern for the NiO/C, the core-shell NiO@Pt and PtC-Etek® catalysts, the last used as reference. The samples exhibited high background intensity indicating a portion of highly disordered material by the presence of amorphous carbon and small particle size. The wide peak at 25.12 ° observed in all samples, was ascribed to the hexagonal carbon plane (003) (PDF-01-075-0444-red). The PtC-Etek® shows peaks related to reflection of Face Cubic Center (FCC) crystal structure from metallic Pt (light-green). For the NiO/C sample, were characterized at least two phases: metallic nickel in FCC structure (black) and α-$Ni(OH)_2$ (Blue). We assume that the presence of α-$Ni(OH)_2$ is related to the reaction of Ni with ethanol during the synthesis. On the other hand, the core-shell sample (NiO@Pt), showed well separate diffraction peaks related to those phases from the core and Pt. This feature suggests a strongly phase segregation, which is consistent with that expected for a core-shell structure. The last, agree with that obtained by electrochemistry (see below), where the presence of Ni species on the surface of nanoparticles, characterized by an oxidation peak around 0.4 V was not observed, instead, only a profile related to Pt was observed. This condition together with XRD observation, make us suppose that nanoparticles with high Pt surface segregation were obtained.

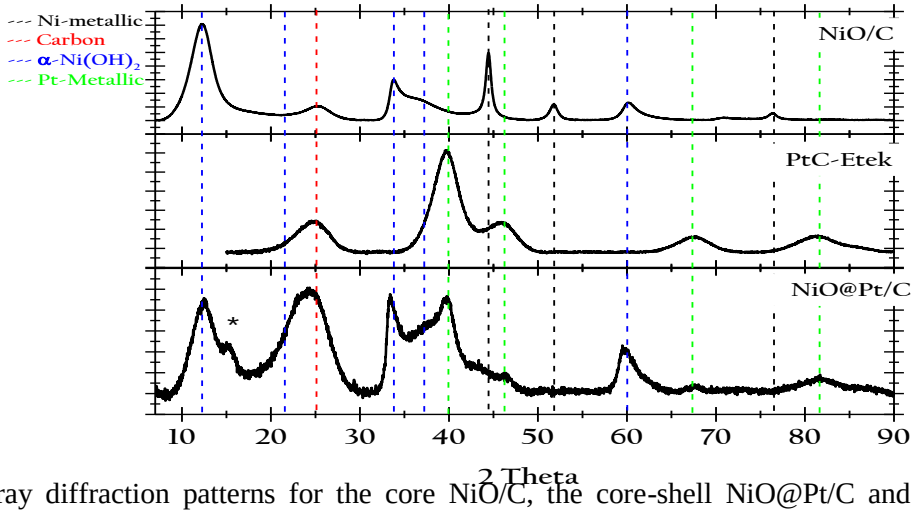

Fig. 2 X-ray diffraction patterns for the core NiO/C, the core-shell NiO@Pt/C and commercial PtC-Etek®. Dashed lines were depicted to clarify the interpretation of different patterns.

3.1.2 Transmission electron microscopy (TEM)

Fig. 3 shows representative low-magnification micrographs and the histograms with the mean particle size distribution determined after evaluation on several regions of the grid. The Fig. 3a depicts dark field scanning transmission electron micrograph (ADF-STEM) for PtC-Etek® catalysts. The Fig. 3b shows a common transmission electron image for NiO@Pt/C. The analysis for both catalysts exhibited spherical morphology with very narrow size distribution for PtC-Etek® 2.45 ± 0.5 nm, however even when the image for NiO@Pt/C shows well distribution 1.73±0.52 nm, they were also found some agglomeration which were not considered during particle size determination, owing to difficulty it implies.

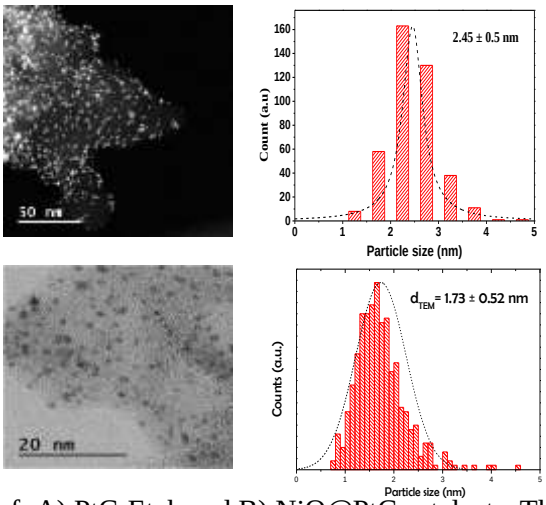

Fig. 3 TEM micrograph of: A) PtC-Etek and B) NiO@PtC catalysts. The histograms show the particle size distribution from several different regions.

3.1.3 Energy dispersive X-ray analysis (EDAX)

Fig. 4a shows images of elemental EDAX mapping on NiO@Pt/C sample. Results suggested a uniform Ni and Pt elemental phase distribution. The amount of Pt obtained was approximately double respect to initially proposed, this to due to impurities of catalysts such as oxides in the core. The oxygen and nickel present in the core have a uniform elemental phase distribution (see Fig. 4b). In the Table 1 are summarized of results real and theoretical of the elemental phase Ni and Pt for the core-shell, and for the core, elemental phase Ni and O_2.

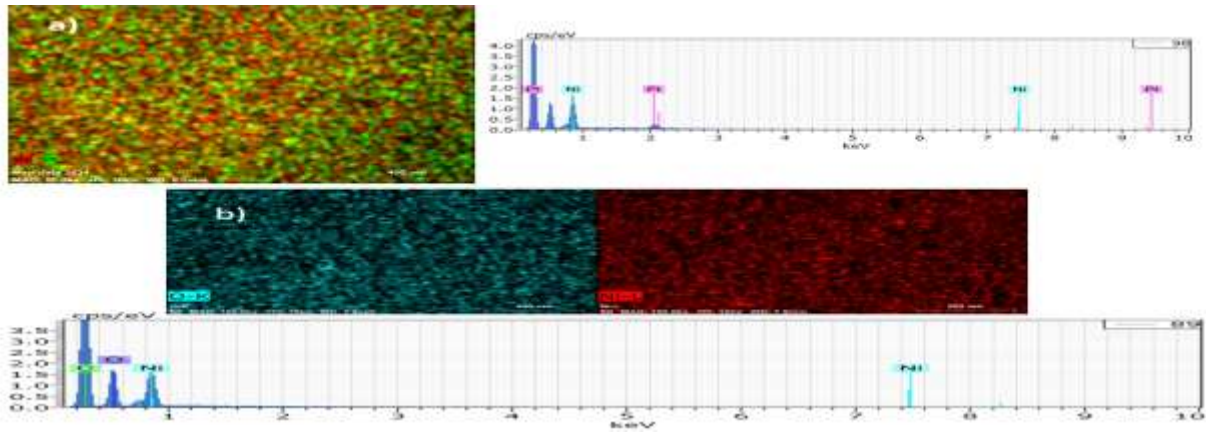

Fig. 4 EDAX mappings of NiO@Pt/C and NiO/C samples: a) Ni and Pt elemental phase distribution, b) Ni and O_2 elemental phase distribution respectively

Table 1 EDAX results real and theoretical of the elemental phase Ni and Pt for the core-shell, and for the core, elemental phase Ni and O2

Sample	EDAX		Theoretical	
NiO@Pt/C	Ni	Pt	Ni	Pt
	70.72±4.4%	29.28±4.4%	85%	15%
NiO/C	Ni	O_2	Ni	O_2
	47.53±2.4%	52.46±2.4%	90%	10%

3.1.4 Raman spectroscopy

Fig. 5 shows the Raman spectra of NiO@Pt/C, was observed that bands of 433 cm^{-1}, 518 cm^{-1} and 1065 cm^{-1} are associated with NiO [16-17]; for the great content support (carbon) the band 1065 cm^{-1} is overlapped. For the carbon, the principal bands are the D, G and 2D at 1330 cm^{-1}, 1595cm^{-1} and 2678-2886 cm^{-1} respectively. The D band represents the amorphous carbon part, the G band is the crystalline part, and the 2D band is the doublet was explained by the 3D graphitic ordering of the crystallites. [18]

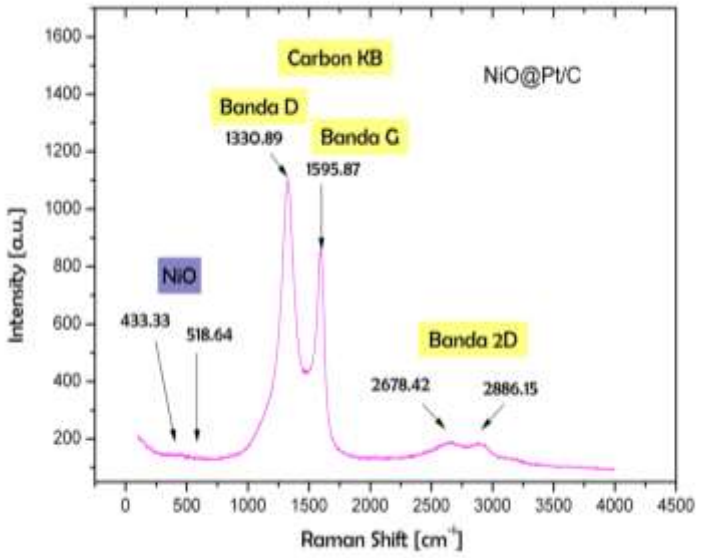

Fig. 5 Raman spectra of NiO@Pt/C

3.1.5 X-ray photoelectron spectroscopy (XPS)

NiO@Pt/C XPS general spectral revealed that the chemical species involucrate (Ni, Pt, C and O_2) as shown in Fig. 6; for this were realized the high resolutions spectra of the Ni 2p, Pt4f, C1s and O1s (Fig. 7). The Shirley method was used for deconvolution of spectra; in the Ni2p XPS spectra was obtained 6 species: the Ni metal, NiO, NiOH (located at 852.3±0.2eV, 853.69±0.2eV and 855.5±0.2eV) and the satellites respectively (located at 858.1±0.2eV, 860.83±0.2eV and 864±0.2eV), the major Ni specie for this case is oxide state; indicating that the core has a thick overlying the nickel metal [19-21]. The Pt4f XPS spectra has a overlapped Ni3p signal therefore the name of this spectra is Pt4f-Ni3p, was obtained 6 species: the Ni metal, NiO, Pt metal, $Pt(OH)_2$ (located at 67.75±0.2eV, 69.2±0.2eV, 71.19±0.2eV and 72.02±0.2eV respectively) and the satellites for the Ni metal and NiO (located at 72.75±0.2eV and 77.8±0.2eV). The Ni specie indicating an interaction with the Pt, the ratio between Ni and Pt is according at so mentioned EDAX. The $Pt(OH)_2$ is referent at hydration of the ambient, this specie overlying the nanoparticles has in minor proportion[22]. For the C1s XPS spectra was obtained 5 contributions: three functional groups (C-O, COH at 286.17±0.2eV and COOH at 288.34±0.2eV), two carbon atoms in different hybridized states (sp2 at 284.44±0.2eV and sp3 at 285.03±0.2eV) and one transition state (π-π^* at 290.7±0.2eV), if has a hybridized state sp2 the transition π-π^* is present, the presence of sp3 indicates the presence of defects in the graphitic structure and finally the presence of functional groups is due to chemical and physical activation [23]. The results proposed in O1s XPS spectra may be oxide species (530.27±0.2eV), hydroxide species (531.89±0.2eV) and absorbed water along with C-O bond (534.39±0.2eV).[19,21]

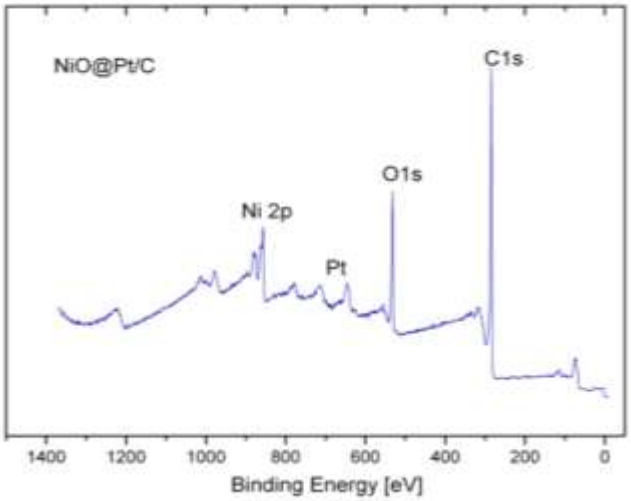

Fig. 6 XPS general spectra of NiO@Pt/C

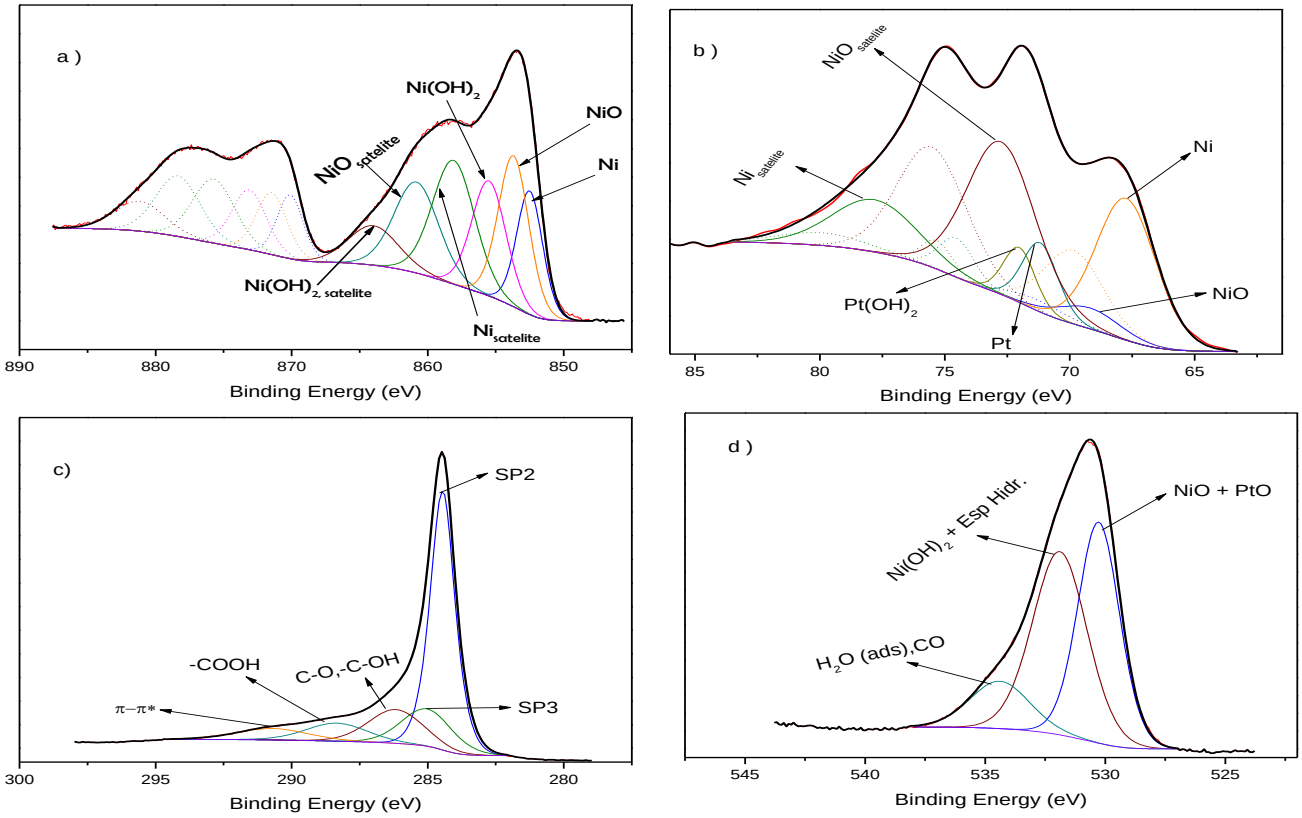

Fig. 7XPS high resolution spectra of NiO@Pt/C sample: a) Ni 2p spectra, b)Pt 4f-Ni 3p spectra, c) C1s spectra, d) O1s spectra

3.2 Electrochemical characterization

The catalysts were electrochemically characterized by cyclic voltammetry (CV) (Fig. 8a). As a systematic procedure, the potential immersion of the working electrode was controlled at 0.1V to avoid possible Ni oxidation during the sample immersion, and then cycled several times between 0.05V and 1.2V until a stable curve was attained. During the first scan was not observed processes assigned to the Ni oxidation, this indicates that the Pt shell completely encapsulate the Ni core. The resolution of the hydrogen adsorption/ desorption region (0.05-0.4V) were not also so well defined and therefore is lower at the Pt features, but this confirms little differences on crystalline surface domain on both catalysts [4,6,11]. In the voltammogram, in the area of the capacitance (localized in the double layer) were observed two peaks associated at process quinine/hydroquinone of the carbon, this process was rationed with the reduction and oxidation of some intrinsic superficial oxide of the carbon black [24-26].

The CO stripping technique was used to determine the specific surface area of the NiO@Pt/C catalysts; considering the charge takes to oxidize the pre-absorbed monolayer of CO is 420μCcm^{-2}[11-12,14]. For CO stripping curves (see Fig. 8b), were recorded in CO-free solution after completely surface saturation by absorbing CO at 0.1V; and cycled several times between 0.5V and 1.2V; the determination of the area was obtained by subtraction of the second sweep. The particle size was calculated by CO stripping as previously reported [27], considering a spherical shape for the catalysts, therefore the particle size estimate was 15.22±2.2 nm. Exist one inconsistency in the particle size determination for this form respect at the other techniques (TEM), because is no takes in consideration the particles agglomeration and/or incomplete stripping of the capping agent during the washing step; by this, exist decreasing the CO adsorption sites in the surface area. Apart the surface analyzed is different for the two cases.

Assessing their electrocatalytic activity for ORR (Fig. 9a) was realized through TF-RDE technique for the catalyst according previously reported Fernando-Godínez et.al [11]. By starting at 1.05 V and scanning the electrode potential negatively, a mixed kinetic-diffusion control region between $0.8 \leq E \leq 0.95$ V is followed by a well defined diffusion-limiting current bellow 0.8 V [11,13,15]. Catalyst electrocatalytic activity towards the ORR is quantified at E= 0.90 V because interferences from mass-transport losses cannot be completely excluded at the higher current densities observed below E= 0.90 V. The electrocatalytic activity of catalysts is best compared by their mass- and area-specific activities using the mass-transport correction for thin-film RDE (equation 1):

$$J_K = \frac{J_L * J}{J_L - J} \qquad (1)$$

The mass-specific activities are estimated via calculation of J_K and normalization to the Pt loading of the disk electrode, and results are summarized in Table 2. The Tafel slopes (Fig. 9b) were fitted the same potential region, and it's important to mention that catalyst was evaluated at least three times even with different electrode Pt loadings to corroborate reproducibility. The values of Tafel slopes were very similar between NiO@Pt/C and Pt-Etek, 81.3mV/dec and 77.71mV/dec respectively. the slight displacement of the Tafel slopes to the right from NiO@Pt/C sample with respect to Pt/C-Etek represents a slight kinetic gain. The inverse of the overall current density (J^{-1}), as a function of the inverse square root of the rotation rate ($\omega^{-1/2}$), known as Koutecky-Levich (equation 2), exist a linear relation between J^{-1} vs. $\omega^{-1/2}$, indicating a first order kinetic of the sample respect to the ORR.

$$\frac{1}{J} = \frac{1}{J_K} + \frac{1}{J_L} + \frac{1}{j_f} = \frac{1}{J_K} + \frac{1}{B\omega^{1/2}} \qquad (2)$$

In agreement with the theoretical Koutecky-Levich slope value, i.e. $B_{th} = 12.63 \times 10^{-2}$ mAcm^{-2} rpm$^{-1/2}$, calculated considering a four-electron transfer process leading to water formation, i.e., $O_2 + 4H^+ + 4e^- \rightarrow 2H_2O$ [11-12-15].

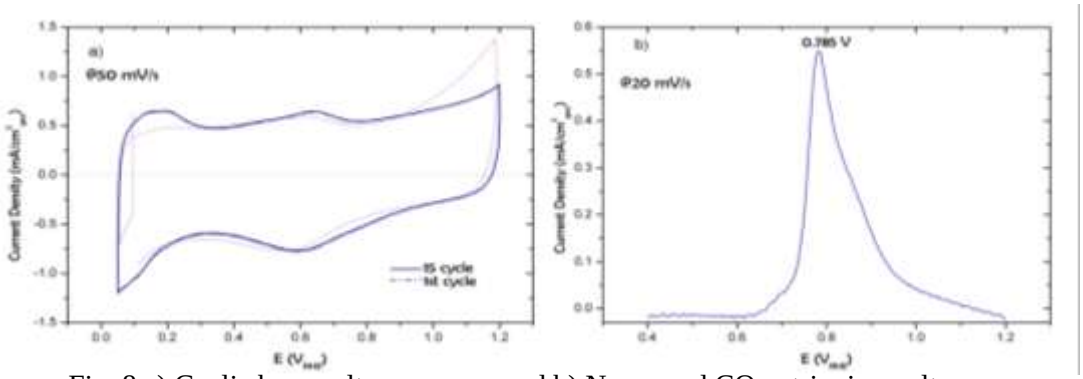

Fig. 8 a) Cyclic base voltammogram and b) N_2-purged CO_{ad} stripping voltammogram of NiO@Pt/C. CV and CO-stripping were carried out in 0.1 M $HClO_4$ at room temperature.

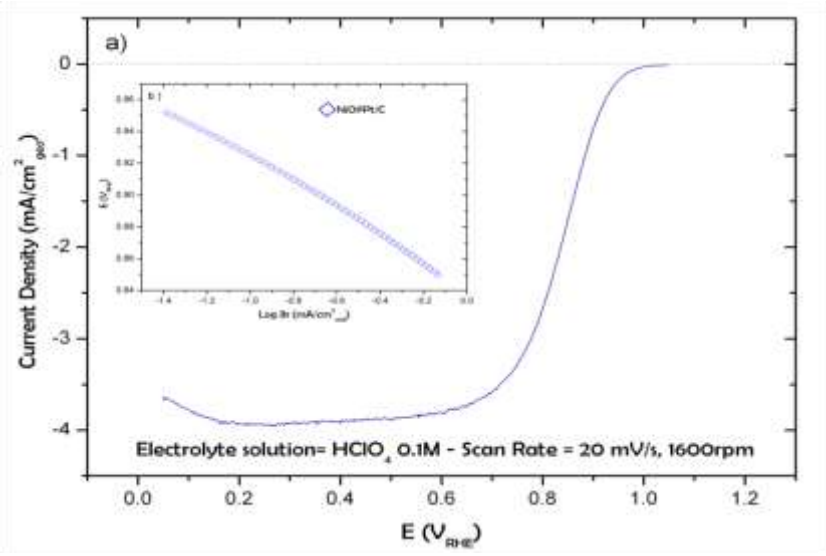

Fig. 9 a) Steady-state polarization curve for the ORR on NiO@Pt/C in O_2 saturated 0.1 M HClO4, b) mass-transfer corrected Tafel plot.

Table 2 Values of kinetic parameters for the ORR on Pt, NiO@Pt/C determined from 1.05 to 0.05 V in negative going sweep at 20 mV s^{-1}. Some data taken from literature are used as reference.

Electrode	$E_{1/2}$ (V)	BC_0 [$mAcm^{-2}{}_{geo}rpm^{-1/2}$]	Tafel slope (mV/dec)	$J_{k0.9V}$ ($mA/cm^2{}_{Pt}$)	$J_{m0.9V}$ (mA/mg_{Pt})	ECSA (m^2/g_{Pt})
Pt	0.89±0.01	0.12±0.004	77.71±9.21	0.21±0.04	180±0.04	77.43±9.59
NiO@Pt/C	0.83±0.01	0.11±0.005	81.43±3.21	0.23±0.04	43.45±2.04	17.63±2.48

4. Summary and perspectives

In summary, well defined and highly disperse NiO@Pt core-shell nanoparticles with size 1.7-15 nm were synthesized by modified Bönnemann procedure using TBAOH as capping agent. XPS, Raman and EDAX showed that the phase present in the core is NiO, but the elemental phase of Ni is present in minor proportion, this indicated that the catalyst is in layers therefore it has form core-shell. The layer or elemental phase that interacts with the Pt is actually the NiO, i.e. Pt-NiO. On the other hand XRD indicate that the NiO, Ni and Pt phases are present, the shifting of Pt reflections to positive diffraction angles indicate that reduced Pt-Pt inter atomic distance on the surface of nanoparticles.

The CV in the O_2 free electrolyte proves that the Pt shell completely encapsulated the Ni core. The electrocatalytic activity of the catalyst has slight kinetic gain for the ORR compared to Pt-Etek under the same measurement conditions; probably this increase is due to the changes in electronic properties of the platinum caused by higher amount of non-noble metal. While the mass activity of ORR is reduced because the particle size that used on the calculations is the obtained by CO stripping. These results reveal that core-shell structure of NiO@Pt could be a good candidate for proton exchange membrane fuel cells.

Acknowledgements

We gratefully acknowledge Ph. D Josue E. Romero, Daniel Bahena and Luis Moreno, for their invaluable assistance in carrying TEM, SEM-EDAX and Raman measurements. The authors acknowledge the support of the National Council of Science and Technology (CONACYT grant FOINS 75/2012) and the University of Texas TAMU-CONACYT project (Alloy nanocatalysts for fuel cell electrodes).

References

[1]Y. Liang, Y. Li, H. Wang, J. Zhou, J. Wang, T. Regier,H. Dai, Co_3O_4 nanocrystals on graphene as a synergistic catalyst for oxygen reduction reaction, ,NATURE MATERIALS, 2011, 10, 780-786

[2] N. M. Markovic´, H. A. Gasteiger, P. N. Ross (Jr.),Oxygen Reduction on Platinum Low-Index Single-Crystal Surfaces in Alkaline Solution:Rotating Ring DiskPt(hkl) Studies, J. Phys. Chem. 1996, 100, 6715-6721

[3]Y. Bing, H. Liu, L. Zhang, D. Ghosh, J. Zhang, Nanostructured Pt-alloy electrocatalysts for PEM fuel cell oxygen reduction reaction, Chem. Soc. Rev., 2010, 39, 2184–2202

[4]G. Wang, H. Wu, D. Wexler, H. Liu, O. Savadogo, Ni@Pt core–shell nanoparticles with enhanced catalytic activity for oxygen reduction reaction, Journal of Alloys and Compounds (2010), 503, L1–L4

[5]D. Jing-Shan,C. Ya-Ting,L. Mei-Hua,Effect of thermal annealing on the properties of Co rich core–Pt rich shell/C oxygen reduction electrocatalyst, Journal of Power Sources (2007), 172, 623–632

[6]L.G.R.A. Santos, C.H.F. Oliveira, I.R. Moraes, E.A. Ticianelli, Oxygen reduction reaction in acid medium on Pt–Ni/C prepared by a microemulsion method,Journal of Electroanalytical Chemistry (2006), 596,141–148

[7]A. Jackson,V. Viswanathan, A.J. Forman,A. H. Larsen,J.K. Nørskov,T. F. Jaramillo ,Climbing the Activity Volcano: Core–Shell Ru@Pt Electrocatalysts for Oxygen Reduction, Chem Electro Chem 2014, 1, 67–71

[8]B. Wang,Review Recent development of non-platinum catalysts for oxygen reduction reaction,Journal of Power Sources 152 (2005) 1–15

[9]H.X. Shen, M.M. Xu, X. Yan, J.L. Yao, S.Y. Han, R.A. Gu, Synthesis and surface enhanced optical properties of multibranched spindle particles and core–shell structures, Colloids and Surfaces A: Physicochem. Eng. Aspects (2010),353 , 204–209

[10]H. Bönnemann,R. M. Richards,Nanoscopic Metal Particles 2 Synthetic Methods and Potential Applications,Eur. J. Inorg. Chem. 2001, 2455-2480

[11]F. Godínez-Salomón, M. Hallen-López, O. Solorza-Feria,Enhanced electroactivity for the oxygen reduction on Ni@Pt core-shell nanocatalysts, international journal of hydrogen energy (2012),37, 14902-14910

[12]J.L. Reyes-Rodríguez, F. Godínez-Salomón, M.A. Leyva, O. Solorza-Feria,RRDE study on Co@Pt/C coreeshell nanocatalysts for the oxygen reduction reaction, international journal of hydrogen energy (2013),38, 12634-12639

[13]Y. Garsany,O.A. Baturina, K.E. Swider-Lyons, S.S. Kocha, Experimental Methods for Quantifying the Activity of Platinum Electrocatalysts for the Oxygen Reduction Reaction Anal. Chem. 2010, 82, 6321–6328

[14]M. Arenz,K. J. J. Mayrhofer,V. Stamenkovic,B. B. Blizanac,T. Tomoyuki,P. N. Ross,N. M. Markovic,The Effect of the Particle Size on the Kinetics of CO Electrooxidation on High Surface Area Pt Catalysts,J. AM. CHEM. SOC. 2005, 127, 6819-6829

[15]U.A. Paulus, T.J. Schmidt, H.A. Gasteiger, R.J. Behm, Oxygen reduction on a high-surface area Pt:Vulcan carbon catalyst: a thin-film rotating ring-disk electrode study,Journal of Electroanalytical Chemistry (2001),495, 134–145

[16]J. Nan, Y. Yang, Z. Lin, In situ photoelectrochemistry and Raman spectroscopic characterization on the surface oxide film of nickel electrode in 30 wt.% KOH solution,Electrochimica Acta (2006), 51, 4873–4879

[17]S.S. Chan, I.E. Wachs,In Situ Laser Raman Spectroscopy of Nickel Oxide supported on y-Al2O3, Journal of Catalysis, 1987, 103, 224-227

[18]N. Larouche, B. L. Stansfield, Classifying nanostructured carbons using graphitic indices derived from Raman spectra, Carbon, 2010, 48, 620-629

[19]M. C. Biesinger, B. P. Payne,L. W. M. Lau,A. Gersonb, R. St. C. Smart, X-ray photoelectron spectroscopic chemical state quantification of mixed nickel metal, oxide and hydroxide systems, Surf. Interface Anal. 2009, 41, 324–332

[20]S.G. Zhang, Y. Hara, S. Suda, T. Morikawa, H. Inoue, C. Iwakura, Physicochemical and electrochemical hydriding-dehydriding characteristics of amorphous $MgNi_x$ (x=1.0, 1.5, 2.0) alloys prepared by mechanical alloying, J Solid Sate Electrochem (2001),5, 23-28

[21]M. C. Biesinger, B. P. Paynec, A. P. Grosvenord, Leo W.M. Laua,c, Andrea R. Gersonb, R. St .C. Smart, Resolving surface chemical states in XPS analysis of first row transition metals, oxides and hydroxides: Cr, Mn, Fe, Co and Ni, Applied Surface Science (2011),257, 2717–2730

[22]C. Battistoni, A. M. Giuliani, E. Paparazzo, F. Tarli, Platinum Complexes of the Methyl Esters of Dithiocarbazic Acid and 3-Phenyld it hiocarbazic Acid, J. CHEM. SOC. DALTON TRANS. 1984, 1293-1299

[23]H. Inoue, K. Hosoya, N. Kannari, J. Ozaki, Influence of heat-treatment of Ketjen Black on the oxygen reduction reaction of Pt/C catalysts, Journal of Power Sources (2012), 220, 173-179

[24]O. Martinez-Alvarez, M. Miranda-Hernández, Characterization of carbon pastes as matrices in composite electrodes for use in electrochemical capacitors, Carbon – Sci. Tech. (2008),1 , 30 - 38

[25]F. Godínez-Salomón, E. Arce-Estrada,M. Hallen-López, Electrochemical Study of the Pt Nanoparticles Size Effect in the Formic Acid Oxidation, Int. J. Electrochem. Sci., (2012), 7, 2566 - 2576

[26]P. S. Guin,S. Das,P. C. Mandal, Electrochemical Reduction of Quinones in Different Media: A Review, International Journal of Electrochemistry, 2011, 1-22

[27]S.A. Grigoriev, P. Millet, V.N. Fateev, Evaluation of carbon-supported Pt and Pd nanoparticles for the hydrogen evolution reaction in PEM water electrolysers, Journal of Power Sources, (2008), 177, 281–285